Theory of backward second-harmonic localization in nonlinear left-handed media

Emmanuel Centeno and Cristian Ciracì
GES UMR-CNRS 5650, Université Montpellier II, Place E. Bataillon, CC074, 34095 Montpellier, France
(Received 23 January 2008; revised manuscript received 8 September 2008; published 2 December 2008)

Recent research on photonic crystals possessing a quadratic nonlinear response has revealed a second-harmonic light localization phenomenon that originates from an all-angle phase matching between counterpropagating Bloch modes at the fundamental and double frequencies [E. Centeno *et al.*, Phys. Rev. Lett. **98**, 263903 (2007)]. In this paper, we develop an electromagnetic theory describing the nature of this parametric light localization, which appears in properly design metamaterials or photonic crystals exhibiting nonlinear left-handed behaviors. We demonstrate that interferences between converging phase-matched and diverging anti-phase-matched waves create a localized second-harmonic wave focused on the pump emitter on the scale of half the wavelength. This light trapping is accompanied by the enhancement of the second-harmonic intensity, which linearly increases with the size of the two-dimensional domain. We finally show that the second-harmonic localization effect previously proposed for GaN photonic crystals can also be obtained with $LiNbO_3$ material.

DOI: 10.1103/PhysRevB.78.235101 PACS number(s): 42.65.Ky, 42.70.Qs

I. INTRODUCTION

Since the pioneering work of Yablonovitch[1] and John,[2] considerable progress has been made on the light control in microstructured materials. The possibility of trapping light on the wavelength scale in periodic index materials, called photonic crystals (PhCs), has opened new investigation fields in both fundamental and applied nano-optics.[3] The localization of light in PhCs is based on the excitation of localized states associated to resonant frequencies that lie within photonic band-gap ranges. In practice, it amounts to locally breaking the symmetry of the crystal by inserting defect lattices. The reduction in the laser threshold or the enhancement of nonlinear processes are some examples of the capacity of PhC microcavities to increase light-matter interactions.[4–6] In particular, efficient second-harmonic generation has been explored in single and dual resonant PhC microcavities.[7–11] This frequency doubling process involves a light localization mechanism at the fundamental and/or at the second-harmonic frequencies that increases the lifetime of photons inside the cavity and thus the conversion efficiency.[12] Besides this approach, efficient frequency doubling based on the phase matching technique between the fundamental field (FF) and the second-harmonic field (SHF) has also been considered in these periodic systems.[13–15] In fact, PhCs are particularly reliable materials for achieving the phase matching condition since their dispersion properties can balance the optical index dispersion of semiconductors.[16] Efficient second-harmonic conversion is obtained when this momentum conservation and the light confinement are simultaneously combined within PhCs.[17–20]

Beyond these localization effects, PhCs and more generally metamaterials have opened new routes for the control of the second-harmonic emission. A second-harmonic superprism effect, which consists in producing large shifts of the SHF propagation direction for small pump field variations, is an example of the smart light-emission control achieved in these systems.[21] More recently, an all-angle phase matching condition has been proposed in 2D PhCs.[22] This isotropic phase matching relaxes the angular dependence of the momentum photon conservation and facilitates the second-harmonic conversion because no specific alignment between the pump and the device is needed in experimental setups. In addition, an original backward SHF emission in nonlinear metamaterials and PhCs has been recently reported underlining the similarity of both systems in achieving nonlinear left-handed (LH) effective properties.[23–26] This counterpropagating emission is obtained when the effective phase indices at the fundamental and double frequencies are opposite. In such a phase matching configuration, the second-harmonic generation process is reversed in comparison to the conventional frequency conversion. Indeed, when the FF and the SHF are phase matched, the associated wave vectors $\mathbf{k}_{\omega}$ and $\mathbf{k}_{2\omega}$ are parallel. Now, because of the left- and right-handed (RH) behaviors of the material at ω and 2ω respectively, $\mathbf{k}_{\omega}$ and the Poynting vector $\mathbf{S}_{\omega}$ are antiparallel at the fundamental frequency while $\mathbf{k}_{2\omega}$ and $\mathbf{S}_{2\omega}$ are parallel at the double frequency. Consequently, $\mathbf{S}_{\omega}$ and $\mathbf{S}_{2\omega}$ are antiparallel leading to a second-harmonic emission propagating in the direction opposite to the fundamental one. These specific electromagnetic properties of such materials that we denote by ω-LH/2ω-RH may be obtained from the effective permittivity and permeability in metamaterials or from the combination of counterpropagating fundamental and second-harmonic Bloch modes in PhCs. Properly designed PhCs can combine the all-angle phase matching condition with left-handed properties leading to generation of second-harmonic localized emission.[22] Unlike light localization effects that rely on photonic band gaps, this nonlinear mechanism involves fundamental and second-harmonic Bloch modes in the photonic conduction bands and thus does not require the existence of defect lattices. Moreover, this parametric localization process distinguishes by two fundamental properties being that the second-harmonic field is focused on the half-wavelength scale and its location is only determined by the emitter position.

In this work, we propose an electromagnetic theory describing this uncommon second-harmonic localization process, initially observed for feasible two-dimensional (2D) PhCs etched in GaN semiconductor.[22] For that purpose, we consider homogeneous left-handed materials presenting a second-order susceptibility tensor. In Sec. II, these concepts

are first applied to one-dimensional (1D) media to allow us to show that second-harmonic localization originates from the interaction of backward phase-matched waves and forward anti-phase-matched waves. Then, we show that in two-dimensional left-handed media, this mechanism enhances the second-harmonic electromagnetic density and focuses the signal at the diffraction limit. In addition, the localized wave position is only determined by the emitter position since this parametric light localization process is achieved in homogeneous media. This theoretical analysis is successfully compared with numerical results obtained from a direct integration of Maxwell's equations based on a finite element method. In Sec. III, conditions for backward second-harmonic localization initially obtained in GaN 2D PhCs are demonstrated for a lithium niobate ($LiNbO_3$) PhC. By taking into account refractive index dispersion of $LiNbO_3$ in the photonic band-structure computation, we show that this material makes it possible to combine the isotropic phase matching condition with left- and right-handed properties at ω and 2ω. Simulations based on a multiple-scattering method confirm that the location of the focused second-harmonic wave is only dependent on the source position within the PhC. Finally, the width of the confinement area is successfully compared with our theoretical predictions.

II. THEORY OF BACKWARD SECOND-HARMONIC LOCALIZATION IN LEFT-HANDED MEDIA

In this section, we focus on homogeneous nonlinear media presenting a second-order susceptibility tensor $\chi^{(2)}$ reduced, for the sake of simplicity, to a single component d_{33}. Without loss of generality our study is restricted to the TM polarization (electric field perpendicular to the propagation plane) and two kinds of homogeneous media are considered:

(i) ω-RH/2ω-RH media, which possess right-handed properties at both ω and 2ω (such as conventional media).

(ii) ω-LH/2ω-RH media, which exhibits left- and right-handed behaviors at ω and 2ω, respectively (these conditions can be achieved in metamaterials or in photonic crystals).

In order to satisfy the phase matching condition, the relative permittivities and permeabilities satisfy the relations $\varepsilon(\omega)=\varepsilon(2\omega)$ and $\mu(\omega)=\mu(2\omega)$ in the ω-RH/2ω-RH media and $\varepsilon(\omega)=-\varepsilon(2\omega)$ and $\mu(\omega)=-\mu(2\omega)$ in the ω-LH/2ω-RH media. In both cases, the right-handed second-harmonic properties are ensured by choosing $\varepsilon(2\omega)>0$ and $\mu(2\omega)=1$. In addition, regardless of the optical properties of the media, the undepleted pump approximation is assumed (weak SHF conversion is considered) so that the FF and SHF satisfy the following equations:

$$\Delta E_z(\mathbf{r},\omega)+k_\omega^2 E_z(\mathbf{r},\omega)=0, \tag{1}$$

$$\Delta E_z(\mathbf{r},2\omega)+k_{2\omega}^2 E_z(\mathbf{r},2\omega)=-4\left(\frac{\omega}{c}\right)^2 d_{33}(\mathbf{r},2\omega)E_z(\mathbf{r},\omega)^2, \tag{2}$$

where the wave vectors of the FF and SH fields satisfy the phase matching condition $\mathbf{k_{2\omega}}=2\mathbf{k_\omega}$.

In Sec. II A, a rigorous theory of the backward second-harmonic localization in one-dimensional homogeneous left-handed media is proposed. This approach is then generalized for two-dimensional structures in Sec. II B.

A. One-dimensional left-handed homogeneous media

We begin with the well-known SHF conversion in a conventional right-handed medium (ω-RH/2ω-RH) of length L illuminated by a pump field at normal incidence. When the phase matching condition is satisfied, the generated intensity $I_{2\omega}^{\mathrm{RH}}$ presents a quadratic growth.[27] In our case, at the output boundary, the intensity is given by $I_{2\omega}^{\mathrm{RH}}(L)=C^2L^2$, where C depends on the FF intensity, d_{33}, ω, and on the optical indices. Consequently, for a pump field propagating toward the positive x direction, the electric SHF is described by a plane wave having an amplitude growing linearly with the distance (the $e^{i\omega t}$ time dependence is assumed),

$$E_z^{\mathrm{RH}}(x,2\omega)=Cxe^{-ik_{2\omega}x}. \tag{3}$$

This behavior is drawn in Fig. 1(a) for a conventional medium (ω-RH/2ω-RH) with positive matched indices at both frequencies. This computation is supported by a finite element method implemented in a commercial software including perfectly matched layers (PML) boundary conditions.[28]

As shown by Shadrivov *et al.*,[25] a more interesting counterpropagating frequency conversion process can be obtained in metamaterials exhibiting a LH behavior. We illustrate this uncommon nonlinear effect in a left-handed slab of length L possessing negative and positive indices at ω and 2ω, respectively, (ω-LH/2ω-RH) embedded in a linear right-handed medium of positive indices equal to $\sqrt{\varepsilon(2\omega)\mu(2\omega)}$ at both frequencies. This choice of surrounding material prevents spurious SHF reflections since at 2ω the optical indices are perfectly matched to the nonlinear slab boundaries. The simulation presented in Fig. 1(a) shows that the SHF is backward generated yielding to a maximal second-harmonic intensity located at the input interface of the slab. In the framework of the undepleted pump approximation, the second-harmonic conversion is simply reversed in the ω-LH/2ω-RH medium and presents a similar conversion efficiency as for the RH one, $I_{2\omega}^{\mathrm{RH}}(L)=I_{2\omega}^{\mathrm{LH}}(0)$. The backward phase-matched SHF can therefore be represented by a wave propagating in the negative x direction with a maximal amplitude reached at the input interface of the slab,

$$E_z^{\mathrm{LH}}(x,2\omega)=C'(L-x)e^{ik_{2\omega}x}. \tag{4}$$

From the equality of the maximal intensities, it can be seen that $|C|=|C'|$. From Eqs. (3) and (4), the simple correspondence $E_z^{\mathrm{LH}}(x,2\omega)=E_z^{\mathrm{RH}}(L-x,2\omega)$ between the SHFs can be made by considering the coordinate transformation $x\rightarrow L-x$ providing that the constants C and C' are linked by a phase term

$$C'=Ce^{-ik_{2\omega}L}. \tag{5}$$

This result is numerically demonstrated by choosing $k_{2\omega}L$ as an odd multiple of π leading then to a phase term equal to -1 [Fig. 1(b)]. Under these conditions, the second-harmonic electric fields oscillate in the LH and RH media in opposite phase, which confirms the existence of the above phase term. Consequently, in the undepleted pump approximation, the

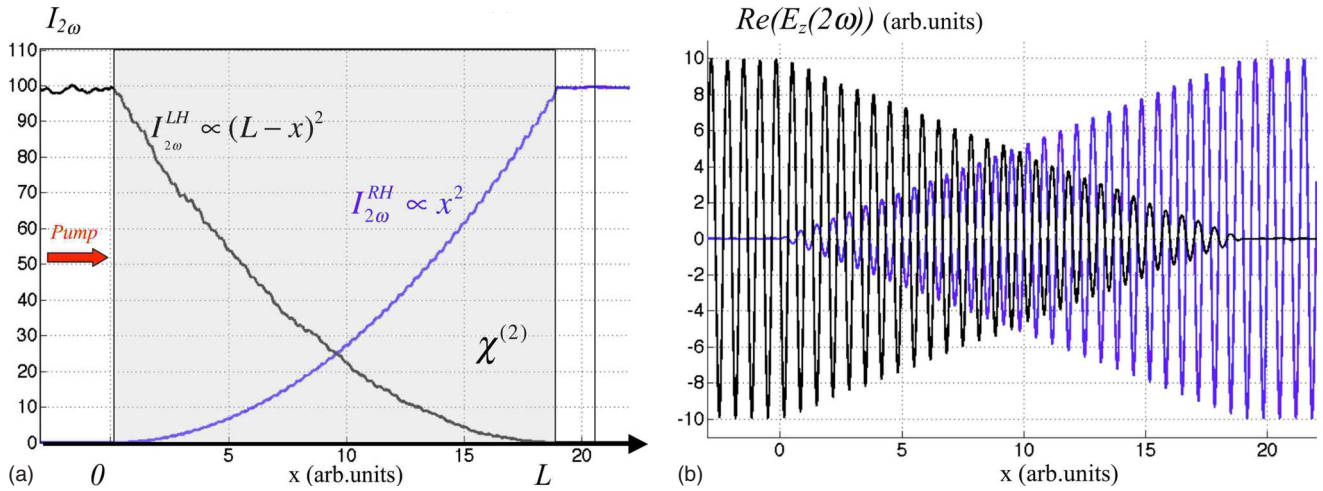

FIG. 1. (Color online) (a) Second-harmonic intensity in a nonlinear medium of length $L=19$ a.u. for a pump source propagating in the positive x direction at the fundamental wavelength $\lambda_F=4$ a.u. Both the pump field amplitude and the second-order susceptibility component d_{33} are normalized to unity. For a conventional medium of indices $n(\omega)=n(2\omega)=3$, the intensity presents a quadratic growth in the positive x direction (blue curve). For a LH medium with $n(\omega)=-n(2\omega)=-3$, the SHF is backward generated with an intensity increasing in the negative x direction (black curve). (b) Real part of the electric SHFs for both RH and LH media (blue and black curves, respectively).

coordinate transformation $x \rightarrow L-x$ makes it possible to deduce the backward conversion in LH media from the conventional process in RH homogeneous media.

These results provide a conceptual basis for the full description of the backward second-harmonic localization effect. The second-harmonic localization appears when the pump source is placed in the nonlinear LH medium and originates from a subtler dynamic. To illustrate this effect, we consider a point source located in the middle of a nonlinear ω-LH/2ω-RH slab of length $2L$. This device can be divided into two symmetric regions, R^- and R^+, corresponding to negative and positive x coordinates, respectively (Fig. 2).

In each region, the Poynting vector of the FF points outward from the source whereas the wave vector $\mathbf{k}_{2\omega}$ points toward it (LH behavior at ω). By virtue of the phase matching condition, the SHF propagates toward the fundamental emitter with both parallel Poynting vectors and wave vectors $\mathbf{k}_{2\omega}$. Considering the above results, the SHFs $\hat{E}_{2\omega}^-(x)$ and $\hat{E}_{2\omega}^+(x)$ in regions R^- and R^+ satisfy the following relations:

$$\hat{E}_{2\omega}^-(x) = C'(L+x)e^{ik_{2\omega}x},$$

$$\hat{E}_{2\omega}^+(x) = C'(L-x)e^{-ik_{2\omega}x}. \quad (6)$$

However, when the wave $\hat{E}_{2\omega}^-(x)$ [resp. $\hat{E}_{2\omega}^+(x)$] propagates in the opposite region R^+ (respectively, R^-) its wave vector $\mathbf{k}_{2\omega}$ is antiparallel to $\mathbf{k}_\omega$, thereby leading to an antiphase matching configuration (Fig. 2). The amplitude of $\hat{E}_{2\omega}^-(x)$ [resp. $\hat{E}_{2\omega}^+(x)$] then remains constant and equal to $C'L$ in the area R^+ (respectively, R^-). In sum, the total SHF in each region is the superposition of a phase-matched SHF having an amplitude growing toward the source and an anti-phase-matched field of constant amplitude,

$$E_{2\omega}^-(x) = C'(L+x)e^{ik_{2\omega}x} + C'Le^{-ik_{2\omega}x} \quad \text{in } R^-,$$

$$E_{2\omega}^+(x) = C'(L-x)e^{-ik_{2\omega}x} + C'Le^{ik_{2\omega}x} \quad \text{in } R^+. \quad (7)$$

In the vicinity of the fundamental source emitter, these fields present similar amplitudes, yielding an interference intensity pattern,

$$I_{2\omega}^-(x) = |C'|^2L^2[1+(1+x/L)^2 + 2(1+x/L)\cos(2k_{2\omega}x)] \quad \text{in } R^-,$$

$$I_{2\omega}^+(x) = |C'|^2L^2[1+(1-x/L)^2 + 2(1-x/L)\cos(2k_{2\omega}x)] \quad \text{in } R^+. \quad (8)$$

The direct simulation supported by the finite element method software confirms this dynamic [Fig. 3(a)]. The comparison

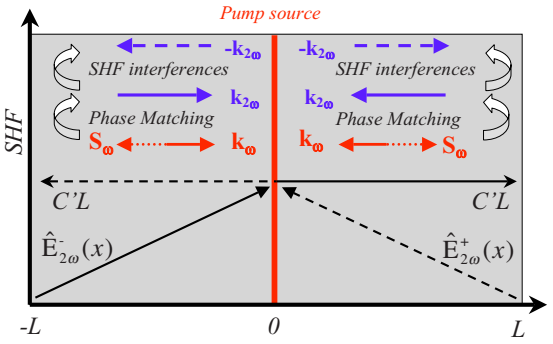

FIG. 2. (Color online) Illustration of the backward second-harmonic localization process. A point source is placed in the center of a nonlinear ω-LH/2ω-RH medium (red line). The FF wave vector $\mathbf{k}_\omega$ is directed toward the emitter position and its Poynting vector $\mathbf{S}_\omega$ points outward. In each region, the amplitude of the backward phase-matched SHF increases toward the pump source. In the opposite regions, these fields propagate in an antiphase matching configuration and thus exhibit a constant amplitude $C'L$. The total SHF is the combination of a backward phase-matched wave and a forward anti-phase-matched wave.

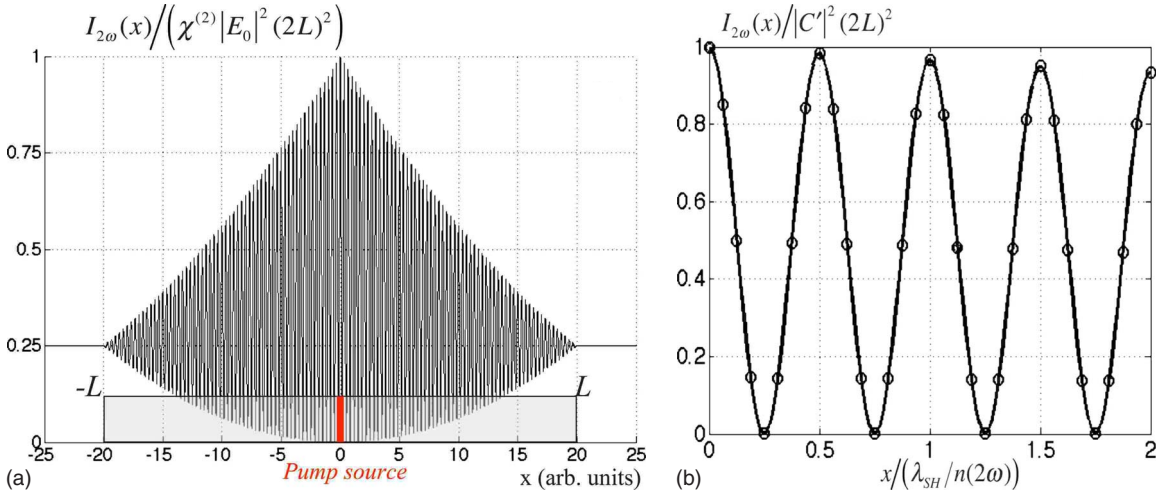

FIG. 3. (Color online) [(a) and (b)] Normalized second-harmonic intensity of the localized SHF field. The maximal intensity is obtained in the center of the ω-LH/2ω-RH medium. (b) Comparison of the intensities derived numerically (solid curve) and analytically from Eq. (8) (circles).

of the analytical solution of Eq. (8) with this computation shows that the 1D backward second-harmonic localization is perfectly described by this theory [Fig. 3(b)]. In accordance with Eq. (8), the generated intensity presents an oscillating pattern of spatial periodicity $\Delta x=\lambda_{SH}/2n(2\omega)$ which is the signature of the interference process between backward and forward waves.

The maximal intensity, $I_{2\omega}(0)=|C'|^2(2L)^2$, is centered on the point source and is equivalent to the intensity reached through a conventional RH medium of length $2L$. Although no specific field enhancement is observed in the one-dimension case, these results show that nonlinear ω-LH/2ω-RH materials are able to trap the SHF within the structure.

B. Two-dimensional left-handed homogeneous media

The study of the second-harmonic localization in 2D LH media follows the same framework as for the 1D version. We first develop the basic concepts of the frequency doubling process in RH media and then use a coordinate transformation to derive the expression of the backward second-harmonic waves. Finally, we conclude with the description of the parametric light localization in LH media.

We start with the second-harmonic conversion in ω-RH/2ω-RH media presenting right-handed properties at both fundamental and double frequencies. A point source emitter is centered inside a circular area of radius R filled by a $\chi^{(2)}$ nonlinear material. In addition, the phase matching condition is assumed to be met along all directions. Although this unusual isotropic phase matching condition is unrealizable in common nonlinear devices, 2D PhCs have proven their ability to obtain it.[22] The electric FF satisfying Eq. (1) is simply the 2D Green's function and considering a $e^{i\omega t}$ time dependence, the FF propagating in the ω-RH medium can then be written as

$$E_z^{\mathrm{RH}}(r,\omega)=E_0H_0^{(2)}(k_\omega r), \tag{9}$$

where r is the radial coordinate, $H_0^{(2)}(k_\omega r)$ is the Hankel function of the second kind, and E_0 is the electric-field amplitude of the source.[29] Although no analytical solution of Eq. (2) can be found in the two-dimensional case, a far-field expression of the SHF can be obtained by considering the asymptotic expression[29] of $H_0^{(2)}(k_\omega r)$ when $k_\omega r\gg 1$,

$$E_z^{\mathrm{RH}}(r,\omega)=E_0\sqrt{\frac{2}{\pi}}\frac{e^{-ik_\omega r}}{\sqrt{k_\omega r}}e^{-i\pi/4}. \tag{10}$$

Solving Eq. (2), we find that the asymptotic solution of the SHF is a plane wave of constant amplitude,

$$E_z^{\mathrm{RH}}(r,2\omega)=Ce^{-ik_{2\omega}r}, \tag{11}$$

where $C=-4|E_0|^2d_{33}/\pi$.

This result reveals an important difference between 1D and 2D second-harmonic generation processes. Actually, unlike the 1D case, the second-harmonic efficiency is almost independent of the size of the 2D RH medium. This behavior is confirmed by the direct simulation presented in Fig. 4(a) and originates from the $1/r$ decay of the fundamental intensity. Indeed, beyond a distance of half the fundamental wavelength, the pump field is almost completely depleted so that the second-harmonic conversion stops.

To improve the second-harmonic near-field description around the source emitter, the electric field is approximated by the following expression:

$$E_z^{\mathrm{RH}}(r,2\omega)=C\sqrt{k_{2\omega}r}H_0^{(2)}(k_{2\omega}r), \tag{12}$$

which converges to the asymptotic expression (11) when $k_{2\omega}r\gg 1$.

We have seen that in 2D RH media the second-harmonic emission is uniformly distributed along all directions and thus limits the conversion efficiency. On the contrary, we will now show that in LH media the all-angle phase matching condition generates 2π azimuth backward second-harmonic waves that constructively add up around the pump emitter. This SHF localization is demonstrated inside a nonlinear ω-LH/2ω-RH disk of radius R presenting LH and RH properties at the fundamental and double frequencies [$\varepsilon(\omega)=-\varepsilon(2\omega)$ with $\varepsilon(\omega)<0$ and $\mu(\omega)=-\mu(2\omega)=-1$]. This 2D

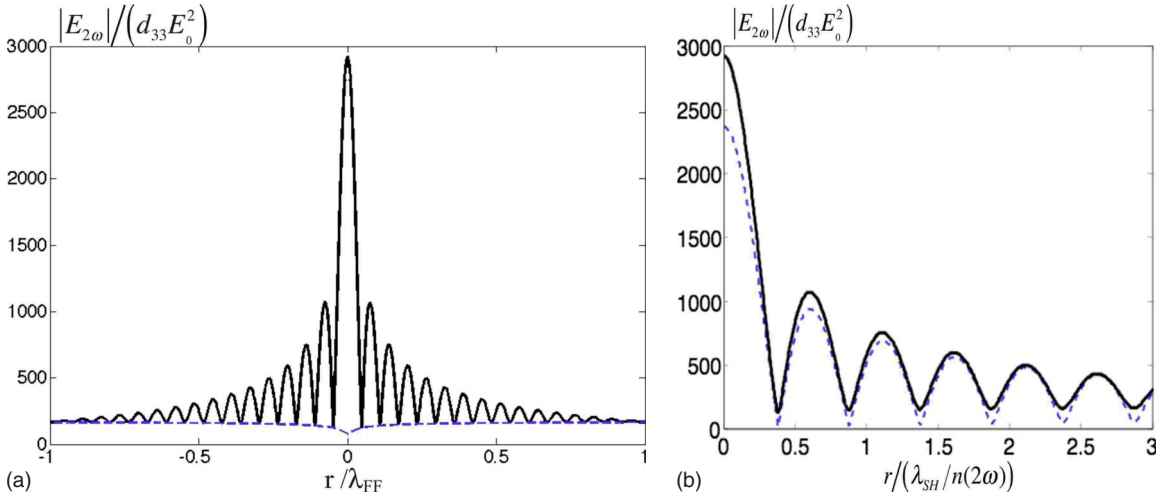

FIG. 4. (Color online) [(a) and (b)] Normalized modulus of the electric SHF for a 2D nonlinear medium of radius $R=1$ (arbitrary units). The pump source is placed in the center of the disk and emits a FF at the wavelength $\lambda_{FF}=R$. For a RH medium phase matched along all direction [the indices are $n(\omega)=n(2\omega)=4$], the SHF reaches a maximal value after a length equal to about $\lambda_{SH}/2n(2\omega)$ (blue dashed curve). For a ω-LH/2ω-RH medium of indices $n(\omega)=-n(2\omega)=-4$, the SHF is enhanced by a factor 17 (black solid curve). (b) Comparison of the SHF obtained with the numerical simulation (black solid curve) and with Eq. (14) (blue dashed curve).

nonlinear medium is embedded in a RH linear one of positive refraction index at both frequencies [$n_\omega=n_{2\omega}=\sqrt{\varepsilon(2\omega)\mu(2\omega)}$]. The perfect optical index matching at 2ω prevents SHF reflections at the boundary of the nonlinear disk. Similarly to the 1D problem, we apply the coordinate transformation $r\rightarrow R-r$ to obtain the expression of the backward SHF in the LH disk,

$$\hat{E}_z^{\mathrm{LH}}(r,2\omega)=C\sqrt{k_{2\omega}R}\sqrt{1-\frac{r}{R}}H_0^{(1)}(k_{2\omega}r). \tag{13}$$

Note that the Hankel function of the second kind is replaced by a function of the first kind to describe the counterpropagating nature of the backward phase-matched wave. The complete description of the second-harmonic localization effect requires introduction of a forward anti-phase-matched field, which propagates outward the energy stored within the left-handed material. This wave appears as a Hankel function of the second kind with a constant amplitude $C\sqrt{k_{2\omega}R}$ equal to the maximal amplitude reached by $\hat{E}_z^{\mathrm{LH}}$ at the center of the disk. The total SHF propagating in the ω-LH/2ω-RH disk can then be written as

$$E_z^{\mathrm{LH}}(r,2\omega)=C\sqrt{k_{2\omega}R}\sqrt{1-\frac{r}{R}}H_0^{(1)}(k_{2\omega}r)+C\sqrt{k_{2\omega}R}H_0^{(2)}(k_{2\omega}r). \tag{14}$$

Since at the boundary of the nonlinear circular medium we have $E_z^{\mathrm{LH}}(R,2\omega)=E_z^{\mathrm{RH}}(R,2\omega)$, no specific second-harmonic emission enhancement is observed outside the left-handed medium [Fig. 4(a)]. On the other hand, the distribution of the SHF is radically different in terms of light confinement. In the vicinity of the source emitter, the interferences between inward and outward waves produce an oscillating intensity pattern that can be approximated by

$$I_{2\omega}^{\mathrm{LH}}(r)=4|C|^2(k_{2\omega}R)J_0(k_{2\omega}r)^2. \tag{15}$$

The minima of the second-harmonic intensity oscillations correspond to the zeros of the Bessel function J_0 and the maximal intensity $I_{2\omega}^{\mathrm{LH}}(r=0)=4|C|^2(k_{2\omega}R)$ is obtained at the pump source location. Therefore, unlike RH materials, the second-harmonic intensity is confined in the device and increases linearly with the radius of the LH disk. The local intensity factor ρ defined by the ratio of the maximal intensities obtained in the LH and RH materials grows linearly with the radius of the nonlinear disk,

$$\rho=\frac{I_{2\omega}^{\mathrm{LH}}(0)}{I_{2\omega}^{\mathrm{RH}}(R)}=4k_{2\omega}R. \tag{16}$$

Direct numerical simulations based on the finite element method confirm this light trapping effect (Fig. 4). The oscillating pattern of the modulus of the SHF is the signature of this interferential process that leads to the intensity enhancement in the nonlinear left-handed medium [Fig. 4(a)]. Figure 4(b) shows the good agreement between the SHF modulus derived from Eq. (14) and the numerical result. It is worth noting that the analytical and the numerical values of local intensity factor, which are, respectively, equal to 200 and 300, indicate that the SHF energy density is enhanced by two orders of magnitude in 2D LH devices.

In the neighboring of the pump source, the combination of two conjugate waves of similar amplitudes creates a second-harmonic standing wave whose confinement is deduced from the expression of intensity given in Eq. (15). The localization radius determined by the first root of the Bessel function is

$$R_{\mathrm{loc}}=\frac{2.40}{2\pi}\frac{\lambda_{\mathrm{SH}}}{n(2\omega)}, \tag{17}$$

whose dimension is smaller than the SHF wavelength [$R_{\mathrm{loc}}=0.38\lambda_{\mathrm{SH}}/n(2\omega)$].

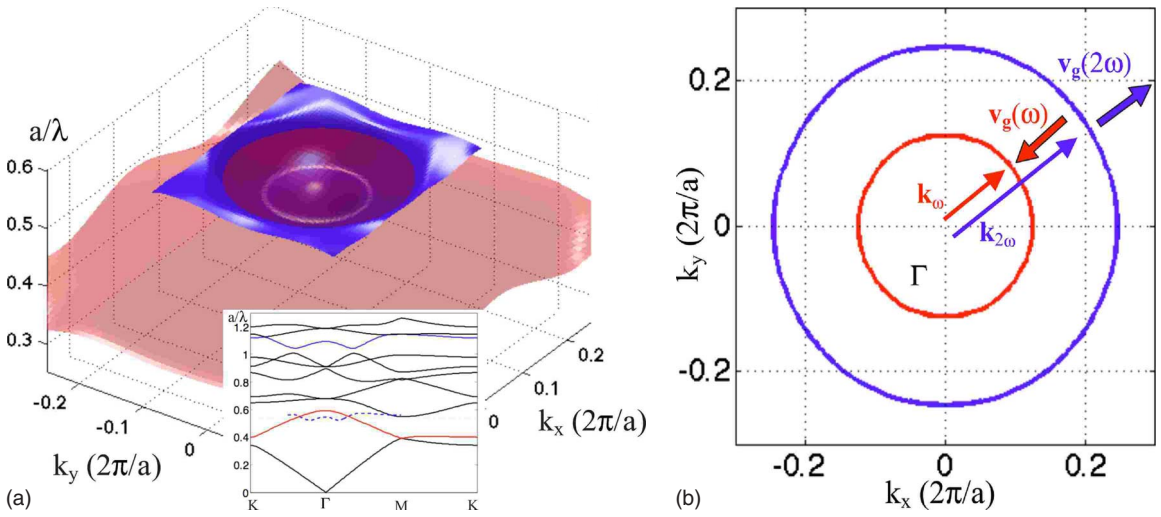

FIG. 5. (Color online) (a) Dispersion surfaces of the second (red) and eighth (blue) bands. The all-angle phase matching condition corresponds to the circular intersection curve of these surfaces. The photonic band structure is shown in the inset. (b) Isofrequency curves computed at $a/\lambda_F=0.545$ (red circle) and at $a/\lambda_{SH}=1.09$ (blue circle). The isotropic phase matching condition is obtained by coupling Bloch modes with antiparallel group velocities (red and blue arrows).

One can remark that this parametric focusing presents some similarities with refocused acoustic signals generated by time-reversal techniques. Indeed, as shown by de Rosny and Fink,[30] time-reversed signals originate from a comparable interference mechanism between converging and diverging waves, which in turn limits the resolution. Here, Eq. (14) shows that in the vicinity of the pump source, the total second-harmonic field is the superposition of two conjugate fields where the backward phase-matched wave can be identified as the time-reversed signal. As for acoustic time-reversed signals, the second-harmonic localized field is diffraction limited with a full width at half-maximum (FWHM) that approaches the half-wavelength [FWHM $=0.36\lambda_{SH}/n(2\omega)$].

III. BACKWARD SECOND-HARMONIC LOCALIZATION IN 2D LITHIUM NIOBATE PHOTONIC CRYSTALS

Although the backward second-harmonic localization process requires very specific conditions, this effect has already been evidenced in the case of a 2D PhCs etched in GaN.[22] The aim of this section is to show that LH phase-matching conditions are not restricted to GaN but can also be met in other nonlinear materials as for example in lithium niobate ($LiNbO_3$). Lithium niobate is known for its nonlinear properties and has been recently used to realize 2D and three-dimensional (3D) PhCs.[31–33] Its strong second-order susceptibility ($d_{33}=43.9$ pm/V) may constitute a striking advantage for generating efficient second-harmonic signals. Here, we consider a 2D PhC consisting of an array of airholes embedded in a $LiNbO_3$ material. The remarkable optical properties of ω-LH/2ω-RH media described previously are found in PhCs when the photonic band structure combines counterpropagating Bloch modes that are phase matched along all directions. These conditions entirely rely on finding PhCs with opposite effective phase indices at ω and 2ω. An effective phase index is associated to an isotropic dispersion surface and its sign is determined by the local surface curvature.[34] Since the hexagonal symmetry facilitates the obtaining of isotropic dispersive relations, a triangular array of airholes of lattice period a and radius $r=0.425a$ is considered. The determination of the suitable lattice period is made in the following way: the operating fundamental frequency is initially fixed to determine the optical index of the dielectric material at ω and 2ω. Then, two sets of band diagrams are computed for each index as a function of the reduced frequency a/λ and are tested against the criteria mentioned previously. This approach makes it possible to deduce the lattice period of the desired structure and can be repeated for different pump frequencies. Let us start with the $LiNbO_3$ refraction indices $n(\omega)=2.16$ and $n(2\omega)=2.25$ corresponding to a fundamental wavelength $\lambda_F=1$ μm. Among the photonic bands, the top of the second and eighth bands are locally isotropic around the Γ point and present opposite curvatures, see the inset of Fig. 5(a). These results are visualized in the surface dispersion diagram of Fig. 5(a) by plotting the eighth band for both half frequencies and wave vectors. The intersection of these surfaces reduced to a circle, which corresponds to the isofrequency curve (IFC) obtained for $a/\lambda_F=0.545$.

The opposite curvatures of these dispersion surfaces provide the necessary ω-LH/2ω-RH properties to the PhC since the group velocity $\mathbf{v}_g(\omega)$ [given by $\nabla_k\omega(\mathbf{k})$] and the Bloch wave vector $\mathbf{k}_\omega$ are antiparallel at ω while $\mathbf{v}_g(2\omega)$ and $\mathbf{k}_{2\omega}$ are parallel [Fig. 5(b)]. Therefore, in the phase matching condition $\mathbf{k}_{2\omega}=2\mathbf{k}_\omega$, the SHF propagates in the direction opposite to that of the FF. Finally, a 2D $LiNbO_3$ PhC of lattice period $a=545$ nm and radius airholes of 232 nm exhibits a LH behavior at the fundamental wavelength $\lambda_F=1$ μm and generates a backward SHF at 500 nm in all directions. Consequently, backward second-harmonic emission or localization effects can be observed when an external pump source illuminates this PhC or when a internal source is considered.[22] In addition, these nonlinear effects can be ex-

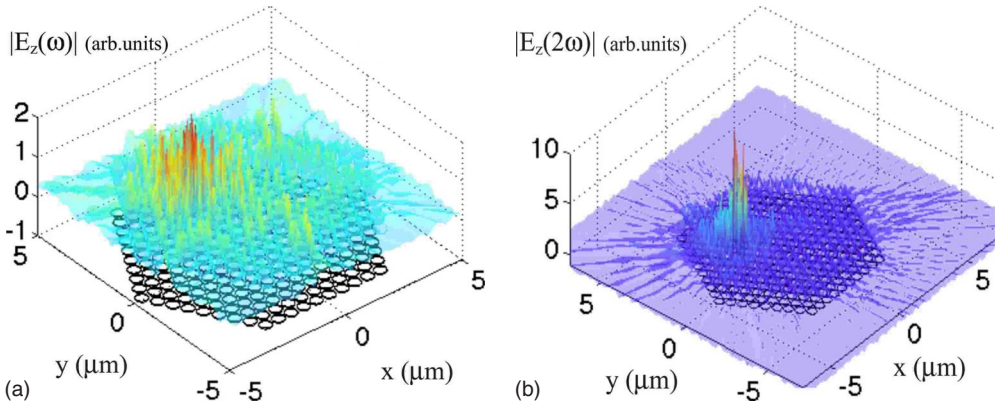

FIG. 6. (Color online) (a) and (b) represent, respectively, the modulus of FF and SHF inside a hexagonal 2D PhC in the case of an off-centered pump source located at $(-1.8;1.2)$ μm. (b) The SHF is localized in the closely vicinity of the pump source emitter.

tended through the entire visible spectrum by keeping the filling factor fixed and scaling the lattice period a accordingly.

The backward second-harmonic localization is now demonstrated for an off-centered source placed inside a finite-size PhC (of lattice period $a=545$ nm and airholes radius 232 nm) and emitting a TM-polarized FF at $\lambda_F=1$ μm. The d_{33} component is chosen perpendicular to the axis of the airholes etched in the (xOy) plane. The fundamental and second-harmonic electric fields are computed using a multiple-scattering method extended to parametric generation process.[35] Since this modal method deals with finite-size 2D PhC, no particular boundary conditions (such as PMLs) are required. Figure 6 shows that the FF spreads over the entire PhC area since it corresponds to a propagating Bloch mode. Conversely, the SHF is confined in a restricted area centered on the pump source location. In accordance with the above theory, the location of the localized SH signal is only determined by the source position. Moreover, the localization radius deduced from this simulation is evaluated to 800 nm which agrees well with the theoretical radius $R_{\mathrm{loc}}=880$ nm derived from Eq. (17) when the index $n(2\omega)$ is approximated by the effective index $n_{\mathrm{eff}}=0.227$ deduced from the IFCs of Fig. 5(b).

Finally, the backward second-harmonic localization observed in PhCs satisfies the principal property reported for homogeneous left-handed media since the source emitter location determines the second-harmonic localization position. However, in periodic index materials, this light localization originates from interferences between converging and diverging Bloch waves instead of cylindrical waves in homogeneous media. These numerical results also prove that feasible PhCs drilled in $LiNbO_3$ materials provide an efficient solution for realizing left-handed materials capable of refocusing a second-harmonic signal on the scale of one wavelength. Since the introduction of a powerful internal source within the device might be difficult in experimental setups, we suggest to extend these results to the case of 2.5D PhCs etched in nonlinear membranes illuminated by an off-plane focused pump beam. The combination of the second-harmonic conversion enhancement already demonstrated in these structures[17,19] together with the LH properties discussed here may open new opportunities for the design of efficient novel compact frequency doublers.

IV. CONCLUSION

We have investigated a second-harmonic light localization effect in $\chi^{(2)}$ nonlinear media exhibiting left- and right-handed behaviors at ω and 2ω, respectively. The theory that we have proposed shows that this localization effect originates from an interference mechanism between backward phase-matched and forward anti-phase-matched waves. This effect combined with an isotropic phase matching condition in two-dimensional left-handed materials yields the focusing of the second-harmonic signal on the scale of half the wavelength. The interferences between converging and diverging second-harmonic waves enhance the local intensity stored around the source emitter but also limit the resolution. In addition, we have shown that the intensity of the localized emission increases linearly with the size of the nonlinear left-handed device unlike right-handed systems where the conversion remains constant. Finally, we have proposed the design of a 2D PhC drilled in $LiNbO_3$ capable of mimicking the necessary left-handed properties to generate localized second-harmonic emission in the visible range of frequencies. We have shown that in accordance with the theory, the position of the focused signal depends only on the location of the pump emitter. We believe that these results open interesting routes for molding the second-harmonic emission in compact photonic crystals or metamaterials and hope that this intriguing localization effect will soon be experimentally explored.

ACKNOWLEDGMENTS

The authors thank the Centre Informatique National de l'Enseignement Supérieur (CINES) of Montpellier (France) for its computing support. The authors also acknowledge J-P Albert for helpful discussions.

[1] E. Yablonovitch, Phys. Rev. Lett. **58**, 2059 (1987).
[2] S. John, Phys. Rev. Lett. **58**, 2486 (1987).
[3] J. D. Joannopoulos, R. D. Meade, and J. N. Winn, *Photonic Crystals: Molding the Flow of Light* (Princeton University Press, Princeton, NJ, 1995).
[4] M. Soljacic and J. D. Joannopoulos, Nature Mater. **3**, 211 (2004).
[5] B.-S. Song, S. Noda, T. Asano, and Y. Akahane, Nature Mater. **4**, 207 (2005).
[6] E. Centeno and D. Felbacq, Phys. Rev. B **62**, R7683 (2000).
[7] D. G. Gusev, I. V. Soboleva, M. G. Martemyanov, T. V. Dolgova, A. A. Fedyanin, and O. A. Aktsipetrov, Phys. Rev. B **68**, 233303 (2003).
[8] F.-F. Ren, R. Li, C. Cheng, H.-T. Wang, J. Qiu, J. Si, and K. Hirao, Phys. Rev. B **70**, 245109 (2004).
[9] B. Shi, Z. M. Jiang, X. F. Zhou, and X. Wang, J. Appl. Phys. **91**, 6769 (2002).
[10] C. Simonneau, J. P. Debray, J. C. Harmand, P. Vidakovic, D. J. Lovering, and J. A. Levenson, Opt. Lett. **22**, 1775 (1997).
[11] A. Di Falco, C. Conti, and G. Assanto, Opt. Lett. **31**, 250 (2006).
[12] V. Berger, J. Opt. Soc. Am. B **14**, 1351 (1997).
[13] V. Berger, Phys. Rev. Lett. **81**, 4136 (1998).
[14] M. Bertolotti, J. Opt. A, Pure Appl. Opt. **8**, S9 (2006).
[15] K. Sakoda and K. Ohtaka, Phys. Rev. B **54**, 5742 (1996).
[16] Y. Dumeige, I. Sagnes, P. Monnier, P. Vidakovic, C. Mériadec, and A. Levenson, J. Opt. Soc. Am. B **19**, 2094 (2002).
[17] A. R. Cowan and J. F. Young, Phys. Rev. B **65**, 085106 (2002).
[18] Y. Dumeige, I. Sagnes, P. Monnier, P. Vidakovic, I. Abram, C. Meriadec, and A. Levenson, Phys. Rev. Lett. **89**, 043901 (2002).
[19] J. Torres, M. Le Vassor d'Yerville, D. Coquillat, E. Centeno, and J. P. Albert, Phys. Rev. B **71**, 195326 (2005).
[20] J. Trull, R. Vilaseca, J. Martorell, and R. Corbalan, Opt. Lett. **20**, 1746 (1995).
[21] E. Centeno, Opt. Lett. **30**, 1054 (2005).
[22] E. Centeno, D. Felbacq, and D. Cassagne, Phys. Rev. Lett. **98**, 263903 (2007).
[23] V. M. Agranovich, Y. R. Shen, R. H. Baughman, and A. A. Zakhidov, Phys. Rev. B **69**, 165112 (2004).
[24] A. A. Zharov, I. V. Shadrivov, and Y. S. Kivshar, Phys. Rev. Lett. **91**, 037401 (2003).
[25] I. V. Shadrivov, A. A. Zharov, and Y. S. Kivshar, J. Opt. Soc. Am. B **23**, 529 (2006).
[26] M. Scalora, G. D'Aguanno, M. Bloemer, M. Centini, D. de Ceglia, N. Mattiucci, and Y. S. Kivshar, Opt. Express **14**, 4746 (2006).
[27] Y. R. Shen, *The Principal of Nonlinear Optics* (Wiley, New York, 1984).
[28] COMSOL MULTIPHYSICS (http://www.comsol.com).
[29] M. Abramowitz and I. A. Stegun, *Handbook of Mathematical Functions* (Dover, New York, 1970).
[30] J. de Rosny and M. Fink, Phys. Rev. Lett. **89**, 124301 (2002).
[31] M. Roussey, M.-P. Bernal, N. Courjal, and F. I. Baida, Appl. Phys. Lett. **87**, 241101 (2005).
[32] M. Roussey, M. P. Bernal, N. Courjal, D. Van Labeke, F. I. Baida, and R. Salut, Appl. Phys. Lett. **89**, 241110 (2006).
[33] G. Y. Zhou and M. Gu, Opt. Lett. **31**, 2783 (2006).
[34] S. Foteinopoulou and C. M. Soukoulis, Phys. Rev. B **67**, 235107 (2003).
[35] E. Centeno and D. Felbacq, J. Opt. Soc. Am. B **23**, 2257 (2006).